A Coplanar Waveguide-Fed Ultra-Wideband Antenna with Single-Band Notched Characteristic using Epsilon-Negative Loading

Saqer S. Alja'Afreh[1,*], Yi. Huang [2]

[1] Department of Electrical Engineering, Mutah University, P.O. Box (7) Zip Code (61710), Al-Karak, Jordan.

[4] Department of Electrical Engineering & Electronics, University of Liverpool, Liverpool, L69 3GJ, United Kingdom.

Corresponding author: [*]eng.saqer-jaa@mutah.edu.jo

Abstract

There is a lot of research being done on ultra-wideband antennas with band-rejection characteristics for specific frequencies, such antennas are used in applications such as the internet of things (IoT) and indoor tracking and localization. This paper presents a single-layer, coplanar waveguide (CPW)-fed, epsilon negative (ENG)-loaded UWB monopole with a single band-rejection characteristic. The proposed antenna represents the first reported ENG-based UWB antenna with a single notched band operation. A 10-dB return loss characteristic (3.1–12 GHz) is achieved by merging five resonances: the zeroth-order resonance (ZOR), first-positive-order resonance (FPOR) of ENG- transmission line (TL), open-slot modes ($\lambda/4$, $3\lambda/4$) and $5\lambda/4$ mode of a shorted monopole. A single-band notch characteristic is achieved between 3.4 and 3.8 GHz by deploying two pairs of radiating structures (two opposite open slots and two opposite L-shaped radiating strips). Opposite currents are excited in each pair, and therefore the total radiated field is canceled at 3.5 GHz notched band. The proposed antenna is printed on a 1.6 mm thick FR4, single-sided copper substrate of dimensions 16 × 20 mm^2. The fabricated prototype is tested, and both simulated and measured results showed that the proposed antenna represents a worthy state-of-the-art UWB antenna.

Keywords: ENG TL; UWB antennas; Notched band UWB; Zero order mode; CPW feed

1. Introduction

In the 1960s, UWB technology saw the light. Due to the unavailability of its infrastructure, UWB did not receive research attention until the late 20th century [1]. In 2002, the Federal Communications Commission (FCC) allowed the use of UWB technology in civil uses. It defined the frequency range of UWB technology. Its frequency band is from 3.1 GHz to 10.6 GHz. Accordingly, UWB technology has witnessed huge research interest from 2002 until 2010 [1]. UWB has re-emerged since 2019 due to its accuracy and reliability in comparison to other technologies. It is integrated inside recent smartphones; it is used in location estimation technology [2,3], indoor tracking systems [4], and internet of things (IoT) applications [5]. According to these new applications, typical characteristics of UWB antennas have been enhanced, such as wide bandwidth, compact size, acceptable gain, and stable radiation patterns [5, 6]. Besides, the frequency spectrum is crowded nowadays, especially, the UWB frequency range (3.1–10.6 GHz). Several licensed and unlicensed wireless technologies have operational frequency bands within the UWB spectrum. For example, sub-6 GHz 5G band (3.4-3.8 GHz), WiFi (5.15–5.825 GHz), and X-band satellite communication (7.25–8.395 GHz). Therefore, finding a UWB antenna that can have the avoidance capability of these wireless applications (notched-band characteristics) represents a new design challenge.

Initially, antenna engineers focused on managing the huge bandwidth criterion. Several works have been published without paying attention to notched-band characteristics [7-16]. Initial research interest has been shown in three-dimensional (3D) planar antenna structures such as planar monopole perpendicular to a large ground plane [7], and planar Inverted-F antenna (PIFA) [8]. However, these structures are no longer preferable with current technology trends toward compact, small, and low-profile hand-portable devices [9]. Printed antennas, such as printed dipoles [10], printed microstrip monopoles [11-14], and printed slot antennas [15-17], are important resources for low-profile UWB antenna research and development. Despite their superior ability to provide UWB operational bandwidth, some have large antenna footprint areas [11-14], while others have complex structures [13, 14, 16]. All these works and others provide a massive pool for bandwidth enhancement techniques such as suitable feeding techniques (proximity-coupled feed [18], and aperture coupled feed [19]), tapering [20] and beveling techniques [21], parasitic elements [9], and metamaterials loading [22-25].

In order to avoid interference from other in-band wireless applications, antenna researchers turned their research attention to finding compact UWB antennas with notched-band characteristics [26–32]. Other in-band wireless applications represented by notched bands include 3.5 GHz WiMax (3.4-3.8 GHz), 5.5 GHz WiFi (5.15-5.85 GHz), and the X-band satellite downlink band (7.1-7.9 GHz). The open literature includes several band rejection techniques such as slots in either ground plane or antenna patch radiators [26], split-ring resonators (SRR) and complementary split-ring resonators (CSRR) [27, 28], electromagnetic bandgap (EBG) structures [29], and parasitic-coupled elements to radiators [30]. However, techniques in [27-29] add complexity to structures, while other solutions [31] increase the antenna footprint area, in which non-compact UWB antennas are produced. Furthermore, changes in either the antenna radiator or the ground plane result in altered radiation patterns [26]. Therefore, the design of a compact UWB antenna with band-notched characteristics is highly recommended.

Due to their unusual physical properties (anti-parallel phase and zero propagation constant) [32], metamaterials (MTM) have been widely deployed in compact antenna design [22, 23, 25]. Normally, metamaterial-loaded antennas are constructed using three kinds of metamaterial transmission lines: (1) composite right/left-handed transmission lines (CRLH TL) [23]; (2) epsilon negative transmission lines (ENG TL) [23, 32]; and (3) mu negative transmission lines (MNG TL) [33]. To the best of our knowledge, the research gap can be summarized as follows: (1) The current state-of-the-art includes only a few metamaterials-loaded UWB antennas, such as UWB antennas based on CLRH TL loading [22] and UWB antennas based on ENG TL loading [21] (2) The published works did not use MTM to find notched band characteristics. Therefore, this work presents the first compact, single-layer UWB antenna based on ENG TL loading with a single notched band characteristic.

This paper is organized as follows: Section 2 presents ENG TL antenna theory. Second, the design methodology (antenna configuration, evolution design process, and parametric study results). The performance of the proposed antenna is evaluated in Section 3 through both the simulated and measured performance parameters results. Section 4 evaluates the proposed antenna design with respect to the current state-of-the-art. Finally, conclusions are drawn in Section 5.

2. Antenna Design Theory and Design Process

2.1 ENG TL Theory

Fig. 1(a) shows a lumped-elements circuit model for a lossy ENG TL. The per unit length lumped elements are as follows: series inductance (L_s), shunt capacitance (C_{sh}), shunt inductance (L_{sh}), shunt conductance (G). The corresponding locations of these circuit elements are annotated in Fig. 2. The corresponding impedance and admittance of the series and the parallel branches are in (1) and (2), respectively.

$$Z' = j\omega L_s \tag{1}$$

$$Y' = G + j\omega\left(C_{sh} - (1/L_{sh})\right) \tag{2}$$

The dispersion relation can be easily derived using Bloch-Floquet unit cell theory to the given unit cell in Fig. 1 [34].

$$\beta(\omega)\rho = cos^{-1}\left(1 - (\omega^2/2\omega_R^2) + (\omega_{sh}^2/2\omega_R^2)\right) \tag{3}$$

Where $\omega_{sh} = 1/\sqrt{L_{sh}C_{sh}}$, $\omega_R = 1/\sqrt{L_sC_{sh}}$, β represents the propagation constant of Bloch wave, and ρ is the length of the unit cell section (the period of ENG TL). Equation (4) represents the resonant condition, in which it is occurred when the total phase on ENG TL satisfies (4), where N is the number of unit cells, l is the physical length.

$$\beta(\omega)\rho = n\pi\rho/l = n\pi/N \qquad \text{n = 0, 1, 2,……., (N-1)} \tag{4}$$

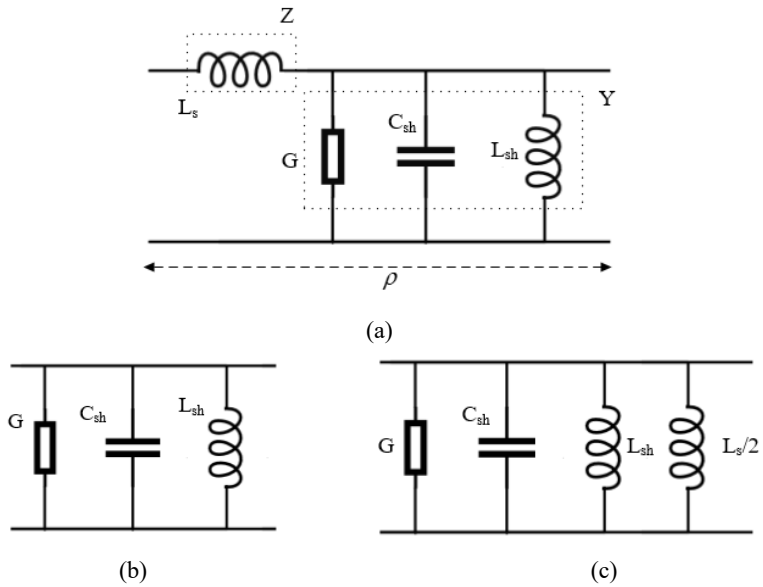

Fig. 1. Equivalent circuit models: (a) Unit cell circuit model of ENG TL, (b) Equivalent circuit of ZOR mode, (c) Equivalent circuit for FOR mode.

Referring to the proposed antenna configuration in Fig. 2, it can be easily noted that the design includes two unit cells (N = 2). Therefore, the range of increment variable (n) is only $n = 0$, and $n = 1$. Substituting these two values in (4) will lead to two resonant conditions, which are: zero-order mode (ZOR) when the total phase equals zero $\beta(\omega)\rho = 0$, and first-order mode (FOR) when the total phase equals $\beta(\omega)\rho = (\pi/2)$. These two conditions are substituted in (3), then equation (3) is solved in-terms of ω:

$$\omega = \begin{cases} \omega_{sh} = \omega_{ZOR} = 1/\sqrt{L_{sh}C_{sh}} & \beta\rho = 0, ZOR\ Mode \\ \omega_{FOR} = \sqrt{2\omega_R^2 + \omega_{sh}^2} = \sqrt{(2/L_sC_{sh}) + (1/L_{sh}C_{sh})} & \beta\rho = \pi/2, FOR\ Mode \end{cases} \quad (5)$$

It can be noted from (5) that the main circuit for ZOR mode is a shunt (G, L_{sh}, C_{sh}) circuit as in Fig. 1(b), while the equivalent circuit of the FOR mode is a shunt (G, C_{sh}, L_{sh}, $L_s/2$) as in Fig. 1(c).

After applying the Theory of microwave transmission line resonators (open-circuited resonators) as described in [35], the basic definition of the quality factor can be used to derive the quality factor (Q) of each resonant mode as follows:

$$Q = 2\pi(Energy\ Stored/Energy\ dissipated\ per\ cycle) \quad (6)$$

$$Q_{ZOR} = (\omega_{ZOR} C_{sh}/G) = \sqrt{(C_{sh}/L_{sh})}\,/G \quad (7)$$

$$Q_{FOR} = \left(\frac{\omega_{FOR} C_{sh}}{G}\right) = \sqrt{C_{sh}((2/L_s) + (1/L_{sh}))}/G \quad (8)$$

As the bandwidth of resonance circuits is inversely proportional with the quality factor, the corresponding bandwidth for each resonant mode will be:

$$BW_{ZOR} \cong G\sqrt{L_{sh}/C_{sh}} \quad (9)$$

$$BW_{FOR} \cong G/\sqrt{C_{sh}((2/L_s) + (1/L_{sh}))} \quad (10)$$

In (10), the total inductance $L_{Parallel}$ represent the equivalent inductance of the parallel connected inductances $L_s/2$ and L_{sh}. $L_{Parallel} = 1/[(1/(0.5L_s)) + (1/L_{sh})]$ Therefore, Eq (10) will be as follows:

$$BW_{FOR} = G\sqrt{L_{Parallel}/C_{sh}} \quad (11)$$

According to (5), (9), and (11), several important relationships can be summarized as follows:

1. Both resonant frequencies (ω_{ZOR}, ω_{FOR}) and their bandwidths are inversely proportional with the square root of the shunt capacitance.
2. The resonant bandwidth of ZOR mode is directly proportional with the square root of shunt inductance.
3. The FOR mode's resonant frequency is inversely proportional to the square root of the resultant parallel inductance (L_{sh} and L_s), whereas its bandwidth is directly proportional to it.

Therefore, these two ENG modes can be merged by finely tuning the aforementioned circuit parameters to form a wideband radiation characteristic. Furthermore, they can be merged together with other radiating resonant modes of a suitable antenna structure to form an UWB antenna.

2.2 Antenna Configuration and Design Process

The detailed configuration of the proposed UWB ENG-loaded antenna is shown in Fig. 2, in which the design cascades two ENG TL unit cells. The design is printed on a single-sided copper FR4 substrate of total thickness about 1.6 mm and dimensions 16 × 20 mm^2. The general configuration is a CPW-fed S-shaped monopole that is loaded with two ENG unit cells. Each unit

cell consists of a series inductance, a shunt inductance, a shunt conductance, and shunt capacitance. As depicted in Fig. 2, the shunt inductance is connected between the monopole radiator and a shorted stub beside the radiator. Shunt capacitors are due to the gap between the radiator and the ground plane, while series inductances are on the radiator. The design is fed by a 50 Ω CPW line. In order to enhance impedance matching for some bands, a 0.65 mm step is made prior to the connection with the radiator. For extra tuning of the lowest radiating mode (quarter wavelength slot monopole), a simple two-finger inter-digit capacitor (IDC) is created between the ground and the slot on the left-hand side of the design. Additionally, this IDC increases the shunt capacitance, which in turn controls ENG TL modes. Finally, the CPW line is excited using a coaxial connector, which is not shown in Fig. 2 for the purpose of clarity of the details.

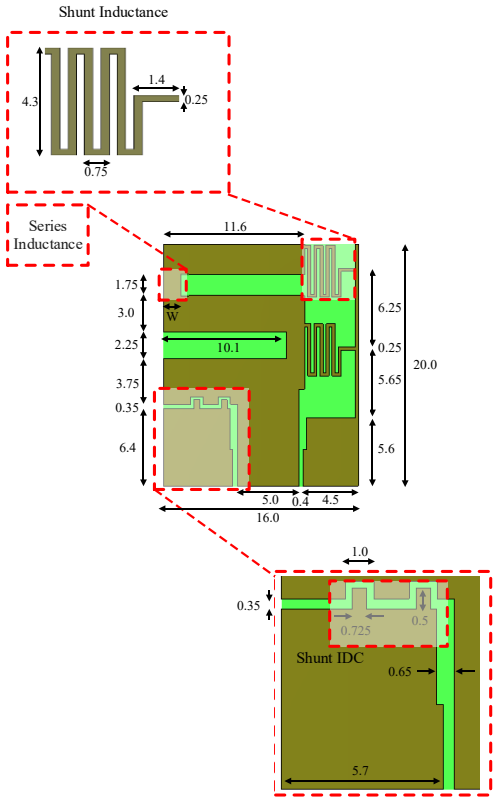

Fig. 2. Proposed UWB antenna configuration. [all units are in mm].

Fig. 3 describes the design evolution process, in which Fig. 3(a) shows that the proposed antenna passed through four design steps (Ant 1, Ant 2, Ant 3, and Proposed). Figure 3(b) depicts the evolution of the reflection coefficient and matching characteristics as a result of each design step. Ant 1 is a CPW-fed, simple S-shaped monopole antenna. It creates two fundamental modes (quarter wavelength monopole and quarter wavelength slot monopole modes). Also, their first-order harmonic modes are excited. However, the entire level of matching within the UWB spectrum is not enough. A grounded stub is added in Ant 2 so that the installation of metamaterial shunt element can be simplified. It is obvious that the addition of this shorted stub deteriorates the matching performance over the entire band of interest. A single unit cell of ENG TL is formed in Ant 3. With this addition, a new resonant mode frequency is created around 4.5 GHz, which represents the ZOR of a single unit cell ENG TL. However, the matching level of the lowest mode around 3 GHz is damaged. Finally, the proposed antenna is created by forming two unit cells of an ENG TL monopole-loaded antenna. This creation adds two extra benefits: (1) it introduces new design parameters that can be used to control the level of matching; and (2) it introduces a new resonant mode (FOR mode of ENG TL) at the lower edge of the band of interest. The proposed design has five resonant modes (open slot monopole, ENG ZOR mode, ENG FOR mode, monopole mode, and open slot mode). The design has a -10 dB impedance bandwidth over (3.1-3.4 GHz) and (3.8-12 GHz), while it has a single notched band characteristic between 3.4 and 3.8 GHz.

Commented [HY1]: Simulated results?

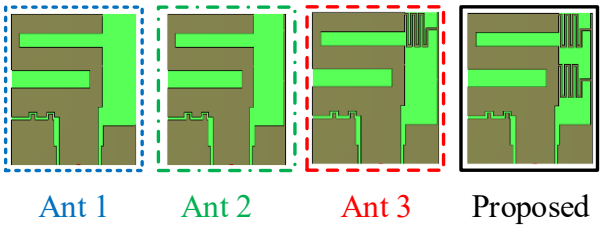

(a)

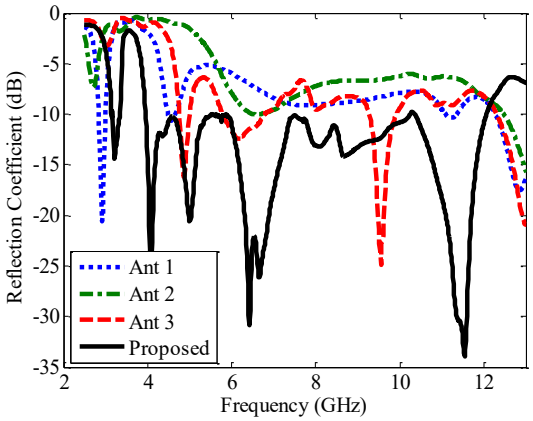

(b)

Fig. 3. Evolution Process, (a) The four steps of the design, (a) Resulting reflection parameter.

In order to understand the excited radiating modes and the rejection mechanism behind the notched band characteristic at 3. 5 GHz, Fig. 4 shows vector surface current distributions at resonant frequencies and the notched band frequency at 3.5 GHz. It shows that an open slot monopole mode (quarter wavelength mode) contributes to the radiation at 3.2 GHz. For the same open slot monopole, its first higher-order harmonic mode ($3\lambda/4$) is radiated at 10.3 GHz. As expected, the excited surface currents are in-phase at ENG TL unit cells at ZOR mode frequency (4.35 GHz), while at FOR resonant mode frequency (4.8 GHz) there is a current null over the unit cells. At 6.35 GHz, the radiation originates mainly from ($5\lambda/4$) monopole mode of the ground stub. Finally, the rejection mechanism at 3.5 GHz can be analyzed as follows: Robust rejection is realized when adjacent currents flow as a transmission line mode (opposite flow) and cancel the radiated fields. This is realized at 3.5 GHz. At this frequency, currents flowing in open slots (between the meandered sections of the S-shaped monopole) are equal in amplitude and in opposite directions. Therefore, their radiated fields cancel each other. In a similar manner, the opposite current patterns exist on the lower left corner of the design and in the upper right corner. Their radiated fields are canceled as well.

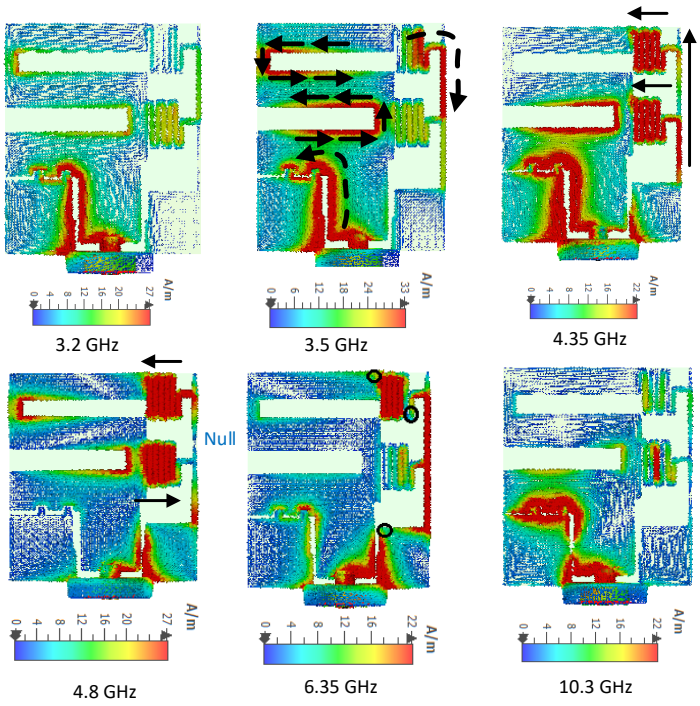

Fig. 4. Vector surface current distributions

In order to validate the achieved results of ENG TL resonant modes, the effects of three important design parameters on the reflection coefficient response are investigated in a parametric study using CST microwave studio. Fig. 5(a) shows that the first and second resonant dips are affected by changing the value of the shunt inductance. These two dips represent resonant frequencies of ZOR and FOR mode, respectively. It can be seen that for a large inductance (solid blue line), both resonant frequencies are decreased, which is already stated in (5). Meanwhile, as the inductance increases, the corresponding 10 dB return loss bandwidth for each mode is increased so that both modes are merged together with our excited modes to form UWB operational bandwidth. Fig. 5(b) shows the effect of the series inductance. It is clearly noted that both the resonant frequency and the operational bandwidth of the FOR mode are affected by changing series inductance value in-terms of strip width (W), and this is already embedded in the presented theory in Section 2.1.

In addition, as the series inductance represents a part of the mirrored open slot, the notched frequency band is also modulated by changing the series inductance. The effect of shunt capacitance is depicted in Fig. 5(c), where the addition of IDC raises the total shunt capacitance. Thus, both ZOR and FOR modes' resonant frequencies are decreased, and this is already proved in (5). Finally, increasing the shunt capacitance (with the IDC case) enhances the whole impedance matching level over the frequency band of interest.

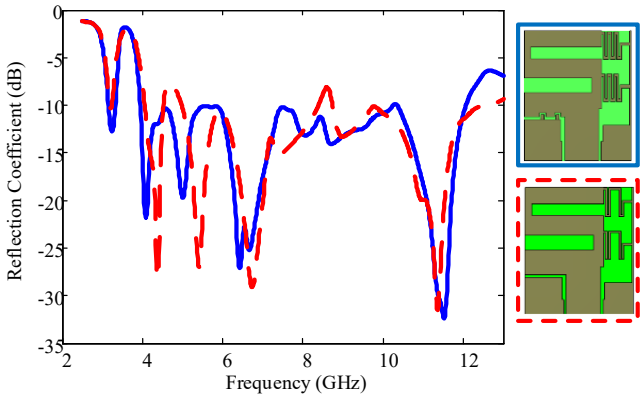

(a)

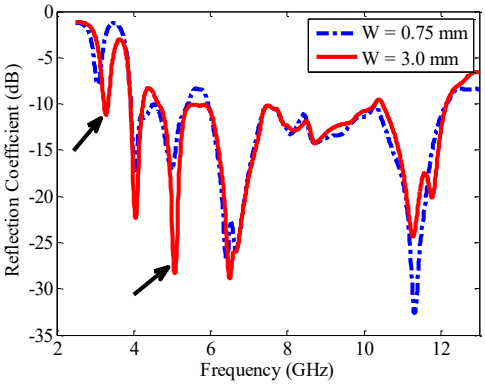

(b)

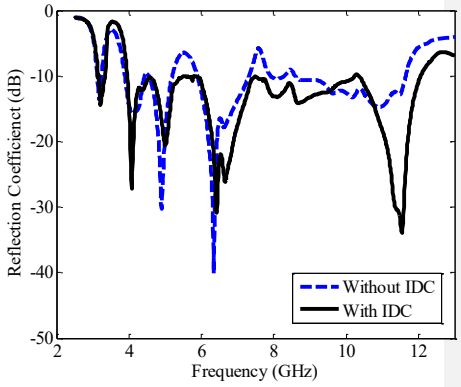

(c)

Fig. 5. Parametric study results, (a) Effect of shunt inductance; (b) Effect of series inductance; (c) Effect of shunt inter-digit capacitor (IDC).

3. Simulated and Measured Results of the Proposed Antenna

A fabricated prototype was tested inside an anechoic chamber at the University of Liverpool. A photo of the prototype inside the chamber is shown in Fig. 6(a). The simulated and measured scattering reflection parameters are attached in Fig. 6(b). Despite a very small discrepancy between the simulated and measured results, they are in good correlation. Based on the -10 dB bandwidth criterion, the design covers the whole UBW spectrum (3.1–12 GHz) with a single-notch band of 400 MHz (3.4–3.8 GHz).

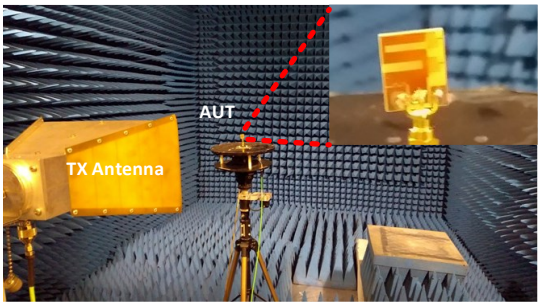

(a)

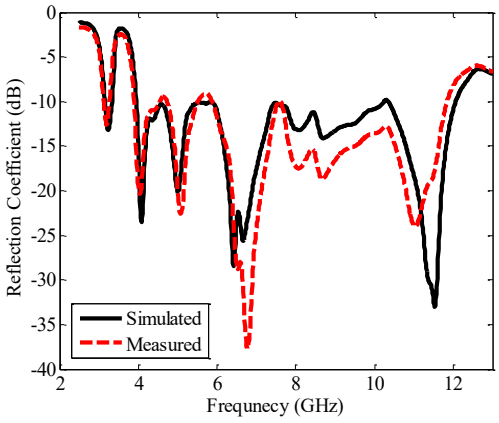

(b)

Fig. 6. (a) Fabricated antenna prototype inside Anechoic Chamber; (b) Simulated and measured reflection coefficients.

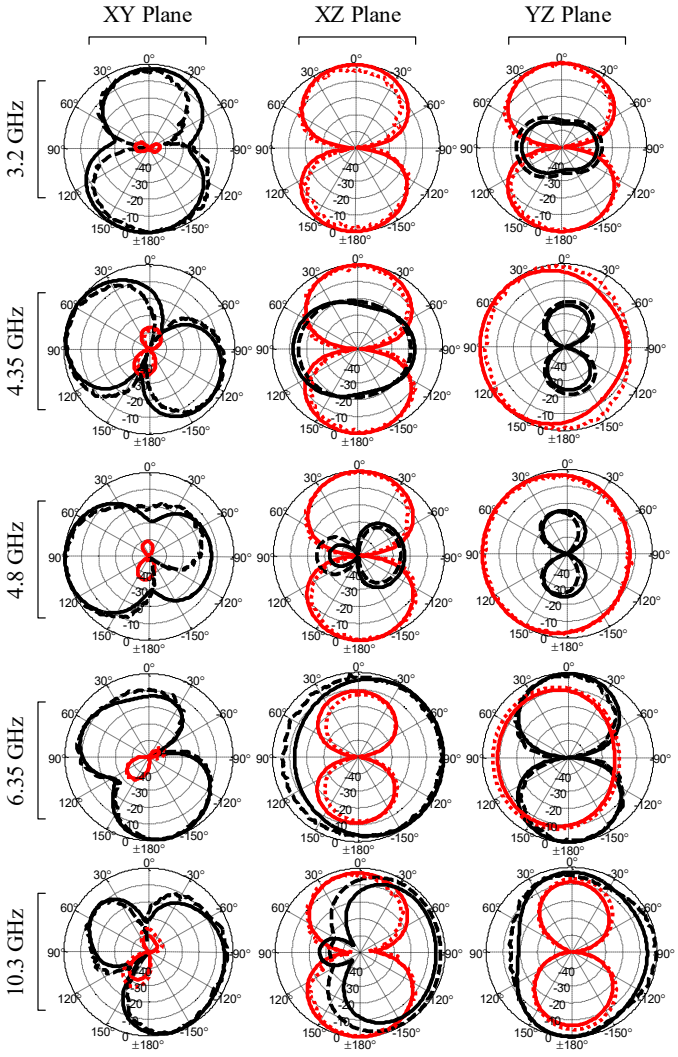

Fig. 7. Normalized simulated and measured far-field patterns in three principal planes (solid lines represent simulated results (Black is E_{φ} and Red is E_{θ}, while the measured ones are in dashed and dotted lines, respectively)

Fig. 7 illustrates the normalized far-field radiation patterns at five resonant frequencies over three principal planes (XY, XZ, and YZ planes). Small differences are existed between the measured

and the simulated results in XY plane and at higher frequencies in both XZ and YZ plane. These differences are due to the fabrication error resulting from the RF cable connectors, soldering process. However, both results are in a good agreement. Furthermore, the measured peak antenna gains are calculated at each resonant frequency and they are found as follows: 1.0 dBi at 3.2 GHz, 1.2 dBi at 4.35 GHz, 1.0 dBi at 4.8 GHz, 2.1 dBi at 6.35 GHz, and 3.0 dBi at 10.3 GHz.

4. Stat-of-the-Art Comparison

Antenna performance metrics are compared to recent state-of-the-art UWB antennas. Table 1 summarizes this comparison. To be fair, all of the works presented are made of FR4 substrate. In comparison to all previous metamaterial-loaded UWB monopoles [22, 23, 25], the proposed design has the smallest size, and it represents the first metamaterial-loaded UWB antenna that has a notch band operation. Even, the size of the proposed design is more compact than conventional unloaded monopole antennas like [12–14, 26, 28, 29]. Some of the open-slot UWB antennas are more compact than the proposed design [15,16], but they fail to provide a notch band operation, which is due to their limited space. Some reported antennas [13, 14] have very large peak gains as they deploy frequency selective surfaces and energy band gap structures (EBG). Nevertheless, such techniques add more complexity to designs. Finally, While the proposed design achieved all aforementioned impacts successfully, it has one limitation, which lies in its low antenna gain and total radiation efficiency. However, it still satisfies the requirements of UWB communications.

Table 1. State-of-the-art comparison

Ref	Antenna Type	Size [mm^3]	Bandwidth (GHz)	Peak Gain (dBi)	# of Notched Bands	Peak Efficiency (%)
[12]	Monopole	26 × 25 × 1.6	3.2-12	4	0	98
[13]	Monopole	61 × 61 × 10	3.05-11.9	9.68	0	95
[14]	Monopole	20 × 25 × 0.2	3.1-10.6	6.53	0	96
[15]	Open Slot	17 × 18 × 1.3	3.05-12	3.36	0	77
[16]	Open Slot	22 × 12 × 0.8	3.1-11	4	2	N.A
[17]	Slot Loop	23.5 × 22 × 1	3.2-16.3	N.A	0	N.A
[22]	ENG Loaded Monopole	22 × 14 × 1.6	3.08-14.1	6.12	0	97
[23]	CRLH TL loaded monopole	33× 20 × 1.6	2.69-9.15	3.37	0	98
[25]	CRLH TL loaded monopole	33× 27 × 1.5	3.2-14	3.9	0	85
[26]	Monopole	40× 34 × 1.6	3.38-13.15	3.88	3	N.A
[28]	Monopole	30 × 25 × 0.8	3.1-10.8	4	3	N.A
[29]	Monopole	25× 16 × 1.5	3.1-12.5	4	1	N.A
[This work]	**ENG Loaded Monopole**	**20× 16 × 1.6**	**3.1-12**	**3**	**1**	**80**

5. Conclusion

In this article, a new, low-profile, ENG-based UWB antenna is proposed with a single-notched band operation for the first time. It covers frequencies between 3.1 GHz to 12 GHz based on S11 < -10 dB bandwidth criterion. A theoretical model is proposed for ENG TL antenna modes. Then, the proposed design is simulated using CST Microwave Studio. Five resonant modes (the zeroth-order resonance (ZOR), first-positive-order resonance (FPOR) of ENG-TL, open-slot modes ($\lambda/4$,

3λ/4), and 5λ/4 mode of a shorted monopole) are created, and merged to form UWB antenna operation. A prototype is fabricated and tested in a free-space environment, and the simulation results are validated by measurement results. Finally, the performance parameters and design parameters of the proposed antenna are evaluated through a comparative study with the current state of the art, which shows that the proposed design represents a good candidate for UWB applications.

References

[1] S. Park, K. Y. Jung, Novel Compact UWB Planar Monopole Antenna Using a Ribbon-Shaped Slo, IEEE Access. (2022) 61951-61959. https://doi:10.1109/ACCESS.2022.3182443

[2] S. Gezici, H. V. Poor, Position Estimation via Ultra-Wide-Band Signals. In Proceedings of the IEEE 2009; 97(2): 386-403. https://doi:10.1109/JPROC.2008.2008840

[3] A. Alabadleh, S. S. Alja'afreh, A. Aljaafreh, K. Alawasa, A RSS-based localization method using HMM-based error correction, Journal of Location Based Services. 12 (2018) 273-285. https://doi:10.1080/17489725.2018.1535140

[2] K. S. Gopalan, A. Bansal, A. R. Kabbinale, Tracking resurgence of ultra-wideband—A standards and certification perspective. In Proc. 14th Int. A. R. Commun. Syst. Netw. (COMSNETS) 2022; 4–8. https://doi:10.1109/COMSNETS53615.2022.9668524

[5] I. Kaur, et al., Annular Ring Ultra Wideband Antenna Integrated With Metallic via Array for IoT Applications. IEEE Access (2022) 73446-73457, https://doi:10.1109/ACCESS.2022.3189573

[6] A. Sarosh, U. Ijaz, S. Naseer, A. Ghaffar, *et al*., A Jug-Shaped CPW-Fed Ultra-Wideband Printed Monopole Antenna for Wireless Communications Networks. Applied Sciences 12 (2022) 821. https://doi.org/10.3390/app12020821

[7] S. -W. Su, J. -H. Chou, K. -L. Wong, Internal Ultra Wideband Monopole Antenna for Wireless USB Dongle Applications. IEEE Transactions on Antennas and Propagation. 55 (2007) 1180-1183, https://doi:10.1109/TAP.2007.893398

[8] H. T. Chattha, Y. Huang, Y. Lu, X. Zhu, An ultra-wideband planar inverted-F antenna. Microwave and Optical Technology Letters. 52 (2010) 2285–2288, https://doi.org/10.1002/mop.25458

[9] S. S. Alja'afreh, Y. Huang, L. Xing, A compact, wideband and low profile planar inverted-L antenna. The 8th European Conference on Antennas and Propagation (EuCAP 2014) 2014; 3283-3286, https://doi:10.1109/EuCAP.2014.6902529

[10] K. Shambavi, Z. C. Alex, Printed Dipole Antenna with Band Rejection Characteristics for UWB Applications. IEEE Antennas and Wireless Propagation Letters. 9 (2010) 1029-1032, https://doi:10.1109/LAWP.2010.2089966

[11] S. Ullah, C. Ruan, M. S. Sadiq, et al., Efficient and Ultra Wide Band Monopole Antenna for Microwave Imaging and Communication Applications. *Sensors (Basel) 20 (2019)*. https://doi:10.3390/s20010115

[12] A. J. Naeem, H. K. Saad, A. S. Daniyal, et al., Design of a compact monopole antenna for UWB applications. Computers. Materials and Continua. 66 (2021) 35-44. https://doi:10.32604/cmc.2020.012800

[13] A. J. A. Al-Gburi, I. B. M. Ibrahim, M. Y. Zeain. Z. Zakaria, Compact Size and High Gain of CPW-Fed UWB Strawberry Artistic Shaped Printed Monopole Antennas Using FSS Single Layer Reflector. IEEE Access. 8 (2021) 92697-92707. https://doi:10.1109/ACCESS.2020.2995069

[14] P. Sambandam, et al., Compact Monopole Antenna Backed With Fork-Slotted EBG for Wearable Applications. IEEE Antennas and Wireless Propagation Letters. 19 (2020) 228-232, https://doi:10.1109/LAWP.2019.2955706

[15] B. Hammache, A. Messai, I. Messaoudene, & T. Denidni, "Compact stepped slot antenna for ultra-wideband applications,"International Journal of Microwave and Wireless Technologies, 14 (2022) 609-615. https://doi:10.1017/S1759078721000726-

[16] H. Yang, X. Xi, Y. Zhao, Y. Tan, Y. Yuan, L. Wang, Compact slot antenna with enhanced bandedge selectivity and switchable band-notched functions for UWB applications. IET Microwaves, Antennas & Propagation 13 (2019) 982–990. https://doi.org/10.1049/iet-map.2018.5832

[17] S.M. H. Varkiani, M. Afsahi, Compact and ultra-wideband CPW-fed square slot antenna for wearable applications. AEU - International Journal of Electronics and Communications. 106 (2019) 108-115. https://doi.org/10.1016/j.aeue.2019.04.024

[18] S. S. Alja'afreh, et al., Ten Antenna Array Using a Small Footprint Capacitive-Coupled-Shorted Loop Antenna for 3.5 GHz 5G Smartphone Applications. IEEE Access. 9 (2021) 33796-33810. https://doi:10.1109/ACCESS.2021.3061640

[19] N. Ghassemi, J. Rashed-Mohassel, M.H. Neshati, A new ultra wideband aperture coupled microstrip antenna. Microw. Opt. Technol. Lett. 51 (2009) 259-260. https://doi.org/10.1002/mop.24004

[20] N. Kumar, K. K. Singh, R. K. Badhai, A tapered feed circular monopole super ultra-wideband (UWB) printed antenna. International Conference on Communication and Signal Processing (ICCSP). (2016) 1943-1946. https://doi.10.1109/ICCSP.2016.7754510

[21] X. N. Qiu, H. M. Chiu, A. S. Mohan, Symmetrically beveled ultra-wideband planar monopole antenna. IEEE Antennas and Propagation Society International Symposium 2A (2005) 504-507. https://doi..1109/APS.2005.1551856

[22] S.S. Al-Bawri, H. Hwang Goh, M.S. Islam, H.Y. Wong, M.F. Jamlos, et al, "Compact Ultra-Wideband Monopole Antenna Loaded with Metamaterial. *Sensors*, 20 (2020) 796. https://doi.org/10.3390/s20030796

[23] B. Niu, Q. Feng, Bandwidth Enhancement of Asymmetric Coplanar Waveguide (ACPW)-Fed Antenna Based on Composite Right/Left-Handed Transmission Line. IEEE Antennas and Wireless Propagation Letters. 12 (2013) 563-566. https://doi:10.1109/LAWP.2013.2260522

[24] T. Shabbir, R. Saleem, S. S. Al-Bawri, M. F. Shafique, M. T. Islam, Eight-Port Metamaterial Loaded UWB-MIMO Antenna System for 3D System-in-Package Applications. IEEE Access. 8 (2020) 106982-10699210. https://doi:1109/ACCESS.2020.3000134

[25] A. Khurshid, J. Dong, R. A. Shi, Metamaterial-Based Compact Planar Monopole Antenna for Wi-Fi and UWB Applications. Sensors. 19 (2019) 5426. https://doi.org/10.3390/s19245426

[26] R. R. Kodali, P. Siddaiah, M. N. Prasad, Design of Quad Band Operational UWB Antenna with Triple Notch Bands Using Meander Line Slot. Progress In Electromagnetics Research. 109 (2022) 63-73. https://doi:10.2528/PIERM22020805

[27] P. R. Sura, K. A. Kumar, Design of Dual-Band Notched UWB Antenna Loaded with Split Ring Resonators for Wide Band Rejection. International Journal of Electronics Letters. (2022) 1-13. https://doi.org/10.1080/21681724.2021.2025437

[28] B. T. P. Madhav, U. Ramya, P. Lakshman, et al., A Triple notch slotted monopole antenna with complementary split ring resonators. International Journal of Computer Aided Engineering and Technology. 15 (2021) 458-474. https://www.inderscienceonline.com/doi/epdf/10.1504/IJCAET.2021.118466

[29] A. Abbas, N. Hussain, M.-J. Jeong, et al., Rectangular Notch-Band UWB Antenna with Controllable Notched Bandwidth and Centre Frequency. Sensors. 20 (2020) 777. https://doi.org/10.3390/s20030777

[30] S. Modak, T. Khan, A slotted UWB-MIMO antenna with quadruple band-notch characteristics using mushroom EBG structure. AEU-International Journal of Electronics and Communications. 134 (2021) 153673. https://doi.org/10.1016/j.aeue.2021.153673

[31] A. A. Gheethan, D. E. Anagnostou, Dual Band-Reject UWB Antenna With Sharp Rejection of Narrow and Closely-Spaced Bands. IEEE Transactions on Antennas and Propagation. 60 (2012) 2071-2076. https://doi:10.1109/TAP.2012.2186221

[32] B. Niu, Q. Feng, P. Shu, Epsilon Negative Zeroth- and First-Order Resonant Antennas with Extended Bandwidth and High Efficiency. IEEE Transactions on Antennas and Propagation. 61 (2013) 5878-5884. https://doi:10.1109/TAP.2013.2281357 .

[33] F. Bilotti, A. Alu, L. Vegni, Design of Miniaturized Metamaterial Patch Antennas With μ -Negative Loading. IEEE Transactions on Antennas and Propagation. 56 (2008) 1640-1647. https://doi:0.1109/TAP.2008.923307

[34] J. H. Park, Y. H. Ryu, J. G. Lee, J. H. Lee, Epsilon negative zeroth-order resonator antenna. IEEE Trans. Antennas Propag. 55 (2007) 3710–3712. https://doi:10.1109/TAP.2007.910505

[35] Pozar D. M., Microwave Engineering. 4th ed. Wiley; 2011.